Intraoperative ^{186}Re-Liposome Radionuclide Therapy in a Head and Neck Squamous Cell Carcinoma Xenograft Positive Surgical Margin Model

Sean X. Wang,[1] Ande Bao,[1,2] Stephanie J. Herrera,[1] William T. Phillips,[2] Beth Goins,[2] Cristina Santoyo,[2] Frank R. Miller,[1] and Randal A. Otto[1]

Abstract

Purpose: Positive surgical margins in advanced head and neck squamous cell carcinoma (HNSCC) have a well-documented association with an increased risk of locoregional recurrence and significantly poorer survival. Traditionally, unresectable tumor is treated with postoperative radiotherapy and/or chemotherapy. However, these therapeutic options can delay treatment and increase toxicity. The potential value of intraoperative injection of liposomal therapeutic radionuclides as a locoregional, targeted therapy in unresectable advanced HNSCC was assessed in a nude rat xenograft positive surgical margin model.

Experimental Design: The therapeutic effects of β-emission rhenium-186 (^{186}Re) carried by liposomes into the tumor remnants in a nude rat squamous cell carcinoma xenograft model were studied. Following the partial resection of tumor xenografts, the animals were intratumorally injected with ^{186}Re-labeled or unlabeled (control) neutrally charged or positively charged 100-nm-diameter liposomes. Tumor size, body weight, hematology, and toxicity were monitored for 35 days posttherapy.

Results: The neutral (n = 4) and cationic (n = 4) liposome control groups showed an increase in tumor growth of 288.0 ± 37.3% and 292.2 ± 133.7%, respectively, by day 15. The ^{186}Re-neutral-liposome group (n = 8) and the ^{186}Re-cationic-liposome group (n = 8) presented with an average final tumor volume of 25.6 ± 21.8% and 28.5 ± 32.2%, respectively, at the end of the study (day 35). All groups showed consistent increases in body weight. No significant systemic toxicity was observed in any of the animals.

Conclusions: With excellent tumor suppression and minimal side-effect profile, the intraoperative use of liposomal therapeutic radionuclides may play a role in the management of positive surgical margins in advanced HNSCC.

The primary management of advanced-stage head and neck squamous cell carcinoma (HNSCC) relies on the complete resection of the tumor. However, the establishment of a histologically sound, margin-free resection is often impossible given the devastating side effects of aggressive surgery and the anatomic proximity to structures such as the carotid artery and the spinal cord. Severe consequences may include loss of voice, swallowing and speech problems, and anatomic deformities (1, 2). Unfortunately, positive margin status, commonly defined as any viable tumor (including carcinoma *in situ* or dysplasia) at the edge of the resected tumor on frozen section or permanent section, is associated with significantly decreased survival (3, 4) due to local or regionally persistent or recurrent disease (2). Traditionally, patients with unresectable HNSCC are treated with postoperative radiation therapy with less than 40% long-term survival (1). With the development of combination chemoradiotherapy, studies have reported a significant increase in overall survival (5); however, the dose-limiting local and systemic toxicity (6–8) of combination therapy leaves more to be desired in terms of better local control and more tolerable side-effect profile.

Given the problem of high local recurrence rate and unbearable toxicity with current therapeutic options for advanced unresectable HNSCC, advancements in treatment should be directed at delivering high local drug concentration while limiting normal tissue toxicity. Liposomes are well known to the medical community, particularly as drug carriers for cancer treatment (9). Most cancer chemotherapeutic agents

Authors' Affiliations: Departments of [1]Otolaryngology-Head and Neck Surgery and [2]Radiology, University of Texas Health Science Center at San Antonio, San Antonio, Texas

Received 9/10/07; revised 2/15/08; accepted 3/10/08.

Grant support: NIH/National Cancer Institute Cancer Center Specialized Programs of Research Excellence grant 5 P30 CA054174-16 and San Antonio Area Foundation, and Frederic C. Bartter General Clinical Research Center Scholar research stipend (S.X. Wang). Rhenium-186 activity was partly supplied by a University of Missouri Research Reactor Sharing grant (U.S. Department of Energy grant DE-FG07-02ID14380).

The costs of publication of this article were defrayed in part by the payment of page charges. This article must therefore be hereby marked *advertisement* in accordance with 18 U.S.C. Section 1734 solely to indicate this fact.

Note: Current address for Stephanie J. Herrera: Department of Otolaryngology-Head and Neck Surgery, University of Texas Health Science Center at Houston, Houston, Texas.

Requests for reprints: Ande Bao, Department of Otolaryngology-Head and Neck Surgery, University of Texas Health Science Center at San Antonio, 7703 Floyd Curl Drive, San Antonio, TX 78229-3900. Phone: 210-567-5657; Fax: 210-567-3617; E-mail: bao@uthscsa.edu.

doi:10.1158/1078-0432.CCR-07-4149

have a large volume of distribution. Liposomes alter the pharmacokinetics and biodistribution of free drugs and/or function as a reservoir for sustained drug release (9). Moreover, in solid tumors, the leaky vasculature and the lack of a well-defined lymphatic system allow i.v. administered liposomes to achieve spontaneous intratumoral accumulation via the enhanced permeability and retention effect (9, 10). The unique properties of liposomes present a viable option for the locoregional delivery of encapsulated therapeutic agents in the positive margins of unresectable HNSCC.

One particularly attractive utilization of liposomes is the encapsulation of therapeutic radionuclides for local injection therapy. Harrington et al. (11) reported intratumoral retention of 15.0 ± 12.3% for ^{111}In-labeled diethylenetriaminepentaacetic-acid liposomes at 96 hours compared with 0.64 ± 0.42% in unencapsulated ^{111}In-diethylenetriaminepentaacetic acid following intratumoral injection in a HNSCC xenograft model. In a similar study, Bao et al. (12) reported a locoregional retention rate of 39.2 ± 10.6% at 20 hours via intratumoral injection of technetium-99m (^{99m}Tc)–labeled liposomes in a HNSCC xenograft model with better intratumoral distribution and a higher local-retention profile than unencapsulated ^{99m}Tc-*N*,*N*-bis(2-mercaptoethyl)-*N*′,*N*′-diethyl-ethylenediamine (BMEDA). These preclinical studies clearly indicate that liposomal radionuclides are capable of achieving sustained local retention via direct injection. To investigate tumor therapy with liposomal radionuclides, a method of encapsulating β-emission therapeutic radionuclides, rhenium-186 (^{186}Re) and rhenium-188 (^{188}Re), with high efficiency, good stability, and convenience has been introduced by Bao et al. (13).

Thus far, previous intratumoral studies have been conducted in an intact tumor model. In a surgical setting, positive margins are the result of maximum resection, and injecting liposomal radionuclides intraoperatively into residual tumor could alter the pharmacokinetics and biodistribution compared with an unresected tumor. Thus, to determine the retention characteristics in an intraoperative setting, we first did an intraoperative biodistribution and retention study, with ^{99m}Tc liposomes of various liposome surface charges and particle sizes injected into nude rat HNSCC tumor model after partial tumor resection. In this previous biodistribution study, we achieved average locoregional and intratumoral retention rates of 65.1 ± 6.8% and 29.5 ± 18.5%, respectively at 44 hours, thus confirming the indication to proceed with therapy study. In the present study, we report the data from our ^{186}Re-liposome intraoperative therapy study in a nude rat HNSCC xenograft model.

Materials and Methods

Preparation of liposomes. Liposomes possessing both glutathione and ammonium (pH) gradients were prepared and characterized with the use of a modified protocol (13). Liposomes with neutral and cationic surface charges and 100-nm diameter were manufactured. Neutrally charged liposomes comprised distearoylphosphatidylcholine (Avanti Polar Lipids), cholesterol (Calbiochem), and vitamin E (molar ratio, 54:44:2). Positively charged liposomes comprised distearoylphosphatidylcholine, 1,2-distearoyltrimethyl ammoniumpropane (Avanti Polar Lipids), cholesterol, and vitamin E (molar ratio, 49:5:44:2). Lipids were co-dried from chloroform to form a lipid film and desiccated overnight. The dried lipid film was rehydrated with 300 mmol/L sucrose in sterile water at 60 mmol/L total lipid concentration and warmed to 55°C followed by an overnight lyophilization. The dried lipid-sucrose mixture was rehydrated with 200 mmol/L glutathione (Sigma) and 300 mmol/L ammonium sulfate (Sigma) in sterile water at 60 mmol/L total lipid concentration, then subjected to five freeze-thaw cycles, followed by sequential extrusion through polycarbonate filters with different pore sizes (2 μm, 1 μm, 400 nm, and 200 nm, two passes each; and 100 nmol/L, five passes) at 55°C (Lipex Extruder, Northern Lipids). After extrusion, liposomes were repeatedly centrifuged at 41,000 rpm for 50 min and washed with 300 mmol/L ammonium sulfate in sterile water thrice to remove any unencapsulated glutathione. Liposome pellets were resuspended in 300 mmol/L ammonium sulfate containing 300 mmol/L sucrose in sterile water at 60 mmol/L total lipid concentration and stored at 4°C until needed.

Following manufacture, liposome sizes were measured with a 488-nm laser light scattering instrument (Brookhaven Instruments) and found to be 109.0 ± 11.1 and 130.5 ± 18.1 nm in diameter for neutral liposomes and cationic liposomes, respectively. Phospholipid content was measured via the Stewart assay (14). Liposomes were also checked for endotoxin levels and bacterial growth (University Hospital Pathology Laboratory, San Antonio, TX). No growth of bacteria was detected within 14-day culture and endotoxin levels were <2.5 EU/mL.

Preparation of ^{186}Re-liposomes. BMEDA (3.0 μL) was added into a vial containing 50 mg glucoheptonate, to which 2.0 mL nitrogen-degassed saline was further added. The mixture was magnetically stirred for 20 min followed by the addition of 240 μL 15 mg/mL stannous chloride solution. After adjusting the pH to 5.0, a 1.0 mL aliquot of the glucoheptonate-BMEDA-stannous solution was placed in a new vial. The vial was then flushed with nitrogen and sealed. ^{186}Re-perrhenate solution (100-120 mCi; University of Missouri Research Reactor) was added to the glucoheptonate-BMEDA-stannous solution and incubated at 80°C for 1 h. After incubation, the ^{186}Re-BMEDA solution was cooled to room temperature and adjusted to pH 7.0. Immediately before radiolabeling, liposomes were eluted with PBS (pH 7.4) through a PD-10 column to remove free ammonium sulfate and create an ammonium (pH) gradient. Eluted liposomes were added into the ^{186}Re-BMEDA solution and incubated for 1 h at 37°C. Labeled ^{186}Re-liposomes were separated from any free ^{186}Re-BMEDA, with PD-10 columns eluted with PBS (pH 7.4). The labeling efficiency of ^{186}Re-liposomes was between 45% and 55%.

HNSCC xenograft model in nude rats. Animal experiments were done according to the NIH Animal Use Guidelines and approved by the University of Texas Health Science Center at San Antonio Institutional Animal Care Committee. During all procedures, the animals were anesthetized with 1% to 3% of isoflurane (Vedco) in 100% oxygen through an anesthesia inhalation machine (Bickford). SCC-4 cell line (American Type Culture Collection) was cultured as described previously (15). Each male *rnu/rnu* athymic nude rat (Harlan) at 4 to 5 wk of age (75-100 g) was inoculated s.c. with 5×10^6 of SCC-4 tumor cells in 0.20 mL of saline on the dorsum at the level of the scapulae. Tumor size was obtained by measuring the length (l), width (w), and thickness (t) of each tumor with calipers. Tumor volumes were subsequently calculated with the ellipsoid volume formula, $V = (\pi/6)lwt$. When the tumor volume reached ~2 to 3 cm^3, which typically occurred between 15 and 17 d after tumor cell inoculation, the tumor-bearing animals were used for study.

Intraoperative therapy of HNSCC xenograft positive surgical margin. On the day of the surgery, the average tumor volume for the neutral liposome control group (n = 4) and cationic liposome control group (n = 4) were 2.6 ± 0.5 and 2.0 ± 0.9 cm^3, respectively. The average preoperative tumor volume for the ^{186}Re-neutral-liposome group (n = 8) and the ^{186}Re-cationic-liposome group (n = 8) were 3.9 ± 0.6 and 3.2 ± 0.7 cm^3, respectively. All instruments were autoclaved, and the sterility of the operating area was maintained. The positive surgical margin model was created via a transverse cutaneous incision directly

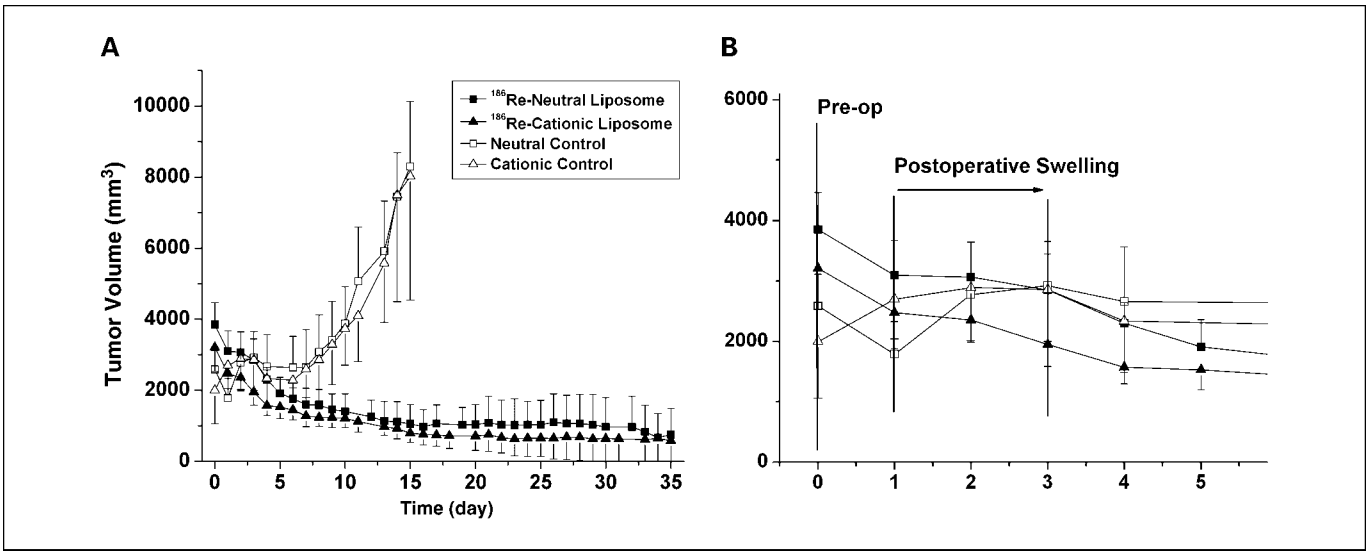

Fig. 1. *A*, average tumor volumes for 35 d from the day of surgical resection for the neutral control, cationic control, ^{186}Re-neutral-liposome therapy, and ^{186}Re-cationic-liposome therapy groups. *B*, average tumor volumes for each group before and for the first 5 d after resection. The two control groups showed progressive tumor growth; in contrast, the therapy groups showed clear and consistent tumor size reduction.

superior to the tumor and by resecting a portion of the tumor while leaving a tumor remnant of 0.5 to 1 cm^3. Each residual tumor was injected with either 0.5 mL ^{186}Re-neutral-liposomes (4.75 ± 0.38 mCi total activity/rat, 13.8 ± 1.3 mg total lipid/kg body weight) or 0.5 mL ^{186}Re-cationic-liposomes (3.95 ± 0.14 mCi total activity/rat, 14.6 ± 1.5 mg total lipid/kg body weight), or 0.5 mL unlabeled control liposomes (12.7 ± 0.7 and 12.8 ± 0.8 mg total lipid/kg body weight for neutral and cationic liposomes, respectively) with the use of 1 mL tuberculin syringes with skin retracted. The skin was closed immediately following surgery and injection with interrupted sutures (3-O silk).

Postoperative follow-up and hematology. Body weight and tumor volume were obtained daily for all rats. Control groups were followed to day 15 postoperatively and then euthanized due to excessive tumor burden by cervical dislocation under deep isoflurane sedation. Therapy groups were followed to day 35 postoperatively and then euthanized. To monitor changes in WBC and platelet levels, blood (500 μL) was collected from the tail vein into tubes containing acid-citrate-dextrose anticoagulant preoperatively and every 3 to 4 d posttherapy until day 35. Blood cell levels were determined by automated counting at the University Hospital Pathology Laboratory (San Antonio, TX).

Intratumoral distribution of ^{186}Re-liposomes via micro–single-photon emission computed tomography/computed tomography imaging. Planar γ-camera images, pinhole-collimator single-photon emission computed tomography (SPECT) images, and computed tomography (CT) images were acquired with a micro-SPECT/CT scanner (XSPECT, Gamma Medica). Static planar images in lateral view were acquired at baseline and at 4, 20, 44, 72, 96, 116, and 140 h after ^{186}Re-liposome administration with parallel hole collimators. During each static image acquisition, a standard ^{186}Re source representing ~5% of the total injected activity per rat was positioned outside the animal but still within the field of view for image quantification.

At 20 h following the intratumoral injection and immediately following static image acquisition, 1-mm pinhole-collimator SPECT images were acquired with the center of the field of view focused on the tumor of each animal (dual detectors, 32 projections/detector, 60 s/projection). The radius of rotation was maintained at around 5.30 cm with a field of view of ~5.00 cm.

SPECT imaging was followed by CT image acquisition (X-ray source: 80 kVp, 280 mA, 256 projections) while precisely maintaining the position of the animal. Software provided with micro-SPECT/CT was used for SPECT and CT image reconstruction, including the SPECT/CT image fusion. SPECT images were reconstructed to produce image sizes of 56 × 56 × 56 with an image resolution of 0.95 mm. CT images were also reconstructed, resulting in image sizes of 512 × 512 × 512 with 0.15-mm image resolution.

Histopathology studies. After the animals were euthanized, the tumor remnant, kidney, liver, and spleen were dissected and fixed in 10% formalin for 48 h and embedded in paraffin; 5 to 6 μm sections were then stained with H&E and assessed in a light microscope. H&E slides were scanned at low resolution with a high-resolution laser scanner, and ×4, ×10, ×20, and ×40 pictures were taken with a digital camera (Canon PowerShot S3 IS).

Data analysis and radiation-absorbed dose calculation. The percentage of injected ^{186}Re activity retained in the tumor and its surrounding tissues, kidneys, and liver over time with the standard source as point of reference was calculated from planar images created by drawing the region of interest with AsiPro software (Siemens Medical Solutions USA, Inc.). The radioactivity with decay correction versus the time curve in each organ for each animal was drawn, and the area from time 0 to 140 h was calculated to obtain the cumulative radioactivity ($\tilde{A}$; mCi-h) in each organ for radiation-absorbed dose calculation.

Most of the radiation energy emitted by ^{186}Re is nonpenetrative radiation mainly from β-ray emission; the nonpenetrative-to-penetrative energy ratio is 16.7 (16). Nonpenetrative radiation from ^{186}Re has an average path length of 1.8 mm (17). If we consider the above characteristics and that only a small fraction of the local dose deposition is due to penetrative radiation energy, we can rationally neglect the radiation-absorbed dose contributed by penetrative radiation from ^{186}Re and only account for the radiation-absorbed doses from nonpenetrative radiation. Because there is a short path length for nonpenetrative radiation, we can also rationally assume that all of the nonpenetrative energies were deposited locally. Based on the above dose calculation model, we can use the following equation to calculate the average radiation-absorbed dose in each organ, including tumor (16):

$$D\ (\mathrm{Gy}) = 7.31\ (\mathrm{Gyg/(mCih)}) \times \frac{\tilde{A}\ (\mathrm{mCih})}{m\ (\mathrm{g})}$$

Here, D is the average radiation-absorbed dose in Gy, $\tilde{A}$ is the cumulative radioactivity in mCi-h calculated as described above, and m is the weight of the organ in grams.

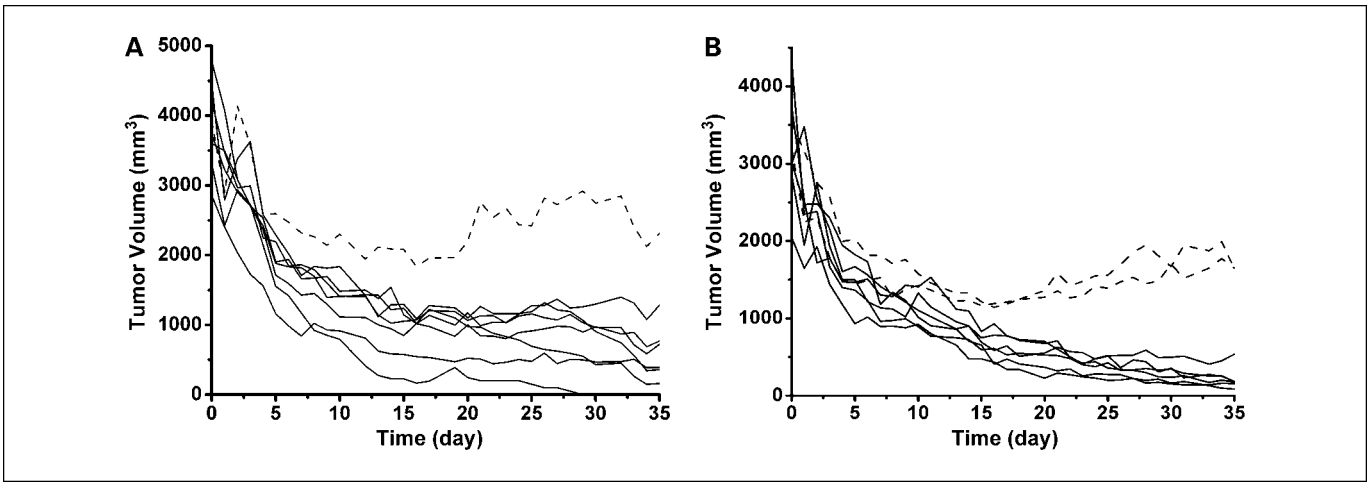

Fig. 2. The progressive tumor volume change for individual rats in the neutral liposome therapy group and the cationic liposome therapy group. Seven of the 8 rats (*solid line*) in neutral liposome therapy group (*A*) showed progressive reduction of the tumor size. One of the 8 rats (*dashed line*) showed continuous tumor size reduction until about day 17, when the tumors progressively enlarged. Six of the 8 rats (*solid line*) in cationic liposome therapy group (*B*) showed progressive tumor size reduction. Two of the 8 rats (*dashed line*) showed continuous tumor size reduction until about day 15, when the tumors progressively enlarged.

To perform radiation-absorbed dose calculation, the tumor weight was calculated from the measured tumor volume at day 3, assuming the tumor density is 1 g/cm^3. For the normal organ weight, the previous organ data [kidneys, 1.974 ± 0.129 g (n = 8) and liver, 10.71 ± 0.67 g (n = 8)] in our ^{99m}Tc-liposome distribution studies were used.

Statistics. Data were summarized and graphed with Origin 7.5 software (Origin Lab). All of the average data were expressed as average ± SD. Paired t tests were used to compare the differences at different time points. One-way ANOVA was used to compare the differences between each group. The correlation between radiation-absorbed dose and tumor size change used linear correlation algorithm. Statistical analysis of significant difference used the standard of 95% confidence interval ($P < 0.05$).

Results

Tumor volume trend. Figure 1A shows the average tumor volume progression for the two ^{186}Re-liposome therapy groups and the two corresponding unlabeled liposome control groups. Final tumor volume is reported as a percentage of the initial tumor volume at the end of the study, and postoperative day 3 is used as the initial reference due to the significant tumor swelling on day 1 and day 2 (Fig. 1B). On day 35, the average tumor volumes of ^{186}Re-neutral-liposome and ^{186}Re-cationic-liposome groups decreased to 25.6 ± 21.8% and 28.5 ± 32.2%, respectively. In comparison, tumors in the neutral and cationic liposome control groups showed rapid growth, with tumor volumes of 288.0 ± 37.3% and 292.2 ± 133.7%, respectively, at day 15.

When individual animals were analyzed, seven of eight animals in the ^{186}Re-neutral-liposome group showed progressive reductions in tumor volume (Fig. 2A) without regrowth, and one of these seven animals had no measurable tumor at day 29. The remaining animal in this group followed a similar trend as the other seven animals for the first 15 days but began to show tumor growth thereafter. The average percent tumor volume change for the seven residual tumors with no regrowth was 20.0 ± 16.3% compared with 64.6% for the one animal with tumor regrowth. Individual tumor volume changes for the eight animals receiving ^{186}Re-cationic-liposomes are shown in Fig. 2B. Six of the eight rats showed consistent tumor volume reduction (12.0 ± 8.2%) without regrowth. Two of the eight rats showed tumor regrowth around day 15 with average tumor volume of 78.0 ± 20% on day 35. In contrast, the two control groups showed no response from the unlabeled liposomes and showed relentless tumor enlargement.

Local retention, distribution, and radiation-absorbed dose. Table 1 illustrates the locoregional level of radioactivity derived from planar images for both the ^{186}Re-neutral-liposome and the ^{186}Re-cationic-liposome groups over the period of study. Both groups showed high local retention rates over 140 hours. Local retention for the ^{186}Re-neutral-liposome group ranged from 86.2 ± 1.0% injected activity at baseline to 18.8 ± 5.3% injected activity at 140 hours. In comparison, the ^{186}Re-cationic-liposome group showed a range of local retention from 81.6 ± 2.7% injected activity at baseline to 28.7 ± 3.6% injected activity at 140 hours. Curve simulations for the

Table 1. Biodistribution of ^{186}Re-liposomes around the locoregional injection site

Therapy group	Baseline	4 h	20 h	44 h	68 h	92 h	116 h	140 h
^{186}Re-neutral-liposomes	86.2 ± 1.0	79.7 ± 2.5	68.4 ± 3.7	49.5 ± 2.0	37.9 ± 4.4	28.6 ± 5.1	22.2 ± 5.9	18.8 ± 5.3
^{186}Re-cationic-liposomes	81.6 ± 2.7	72.1 ± 5.3	62.7 ± 6.5	51.3 ± 4.6	42.8 ± 3.6	36.6 ± 3.0	32.6 ± 3.3	28.7 ± 3.6

NOTE: Data are expressed as mean % injected activity ± SD.

Table 2. Locoregional clearance characteristics of % injected activity after intraoperative injection of ^{186}Re-neutral-liposomes and ^{186}Re-cationic-liposomes

Liposome	Immediate clearance (%)	Phase I clearance (%), $T_{1/2}$	Constant retention (%)	R^2
^{186}Re-neutral-liposome	13.8	78.4, 48.95 h	7.6	0.999
^{186}Re-cationic-liposome	18.4	56.5, 42.04 h	23.9	0.995

locoregional retention of both therapy groups fit a first-order exponential decay model (R^2 = 0.999 and 0.995, respectively), with the following general formula:

$$y = y_0 + A_1 e^{-x/t_1}$$

where y_0 represents the Y offset (i.e., the percentage of constant retention activity other than the cleared components following the exponential decay mechanism) and A_1 represents the percentage of activity that was cleared with a constant of t_1 for each type of ^{186}Re-liposomes. Subsequently, the half-clearance times correlated with the percentage of radioactivity of A_1 is $t_1 \times 0.693$.

Table 2 outlines the clearance characteristics of the two ^{186}Re-liposome therapy groups based on the simulated clearance function described above. There were 13.8% and 18.4% injected activity leaving the local area within a few minutes and distributing systemically to ^{186}Re-neutral-liposome and ^{186}Re-cationic-liposome groups, respectively. For both groups, the locally remaining radioactivity displayed a stable, long-term retention with a half-clearance time of >40 hours. ^{186}Re-cationic-liposomes showed greater constant retention, which may be due to their improved affinity for the tumor tissue. At 140 hours, the ^{186}Re-cationic-liposomes had significantly higher % injected activity compared with the ^{186}Re-neutral-liposomes ($P < 0.001$; Table 1).

Table 3 shows the initial activity (mCi) injected into each animal and the total radiation-absorbed dose (Gy) received by the tumor in each animal during 140 hours. The ^{186}Re-cationic-liposome group received an average absorbed dose of 801.9 ± 184.9 Gy in tumor compared with 617.9 ± 187.0 Gy for the ^{186}Re-neutral-liposome group over the period of 140 hours.

Figure 3 shows the micro-CT, pinhole-collimator SPECT, and fusion images of the HNSCC tumor–bearing rats acquired 20 hours after intraoperative injection of the ^{186}Re-liposomes into the residual tumor. In the ^{186}Re-cationic-liposome rats, the radioactivity was located almost exclusively around the area of the tumor with little peritumoral extravasation, whereas the rats injected with ^{186}Re-neutral-liposomes showed extensive subcutaneous spread of the activity along the lateral aspects of the torsal and forelimbs. The behavior observed with ^{186}Re-neutral-liposomes correlates to the observed recoverable skin ulceration in a few animals treated with ^{186}Re-neutral-liposomes. However, the diffusion of ^{186}Re-neutral-liposomes through the cavity may track the passage of tumor cell local metastasis, which could emerge as a potential advantage of applying ^{186}Re-neutral-liposomes in intraoperative therapy.

Systemic organ retention and dose. Figure 4 illustrates the % injected activity for kidney and liver based on the planar γ-camera images of the animals acquired from baseline until 140 hours after the initial injection of the ^{186}Re-liposomes. The highest average liver % injected activity for the ^{186}Re-neutral-liposome and the ^{186}Re-cationic-liposome animals were 1.7 ± 0.1% at 20 hours and 1.6 ± 0.2% at 4 hours, respectively. The total liver radiation-absorbed dose received by the ^{186}Re-neutral-liposome and the ^{186}Re-cationic-liposome animals were 4.3 ± 0.2 and 3.5 ± 0.1 Gy, respectively. The maximum average kidney % injected activity for the ^{186}Re-neutral-liposome and the ^{186}Re-cationic-liposome animals were 12.1 ± 1.5% and 8.4 ± 1.3%, respectively, at 92 hours. The radiation-absorbed doses received by the kidneys for the ^{186}Re-neutral-liposome and the ^{186}Re-cationic-liposome groups were 149.6 ± 11.3 and 101.6 ± 15.5 Gy, respectively. The radiation-absorbed dose in nude rats would translate to ~1 Gy in humans whose kidneys are ~150 times the size of rat kidneys. This estimated value will be significantly less than the kidney dose limit of 27 Gy in radiation therapy (18).

Body weight growth and hematology. Figure 5A shows the body weight growth trend for all study groups. The control groups showed steady body weight gain beginning on postoperative day 1. Both ^{186}Re-liposome therapy groups

Table 3. The initial activity (mCi) injected into each animal, the radiation-absorbed dose (Gy) received by each animal, and their percentage of tumor volume at day 35 compared with day 3

	^{186}Re-neutral-liposomes			^{186}Re-cationic-liposomes		
	Injected activity (mCi)	Radiation-absorbed dose (Gy)	Tumor volume (%)	Injected activity (mCi)	Radiation-absorbed dose (Gy)	Tumor volume (%)
Rat 1	5.1	472.0	10.9	4.1	1188.4	9.9
Rat 2	4.8	977.3	27.8	4.3	883.3	22.5
Rat 3	4.8	620.5	8.6	3.5	616.0	28.3
Rat 4	4.6	596.9	64.1	4.1	614.9	47.4
Rat 5	4.3	551.3	10.0	3.7	827.7	26.7
Rat 6	4.5	503.0	3.7	4.1	688.4	5.3
Rat 7	4.3	416.4	11.0	3.9	804.9	64.6
Rat 8	5.6	806.2	91.8	3.9	792.1	0.0
Average	4.8 ± 0.4	617.9 ± 187.0	28.5 ± 32.2	3.9 ± 0.2	801.9 ± 184.9	25.6 ± 21.8

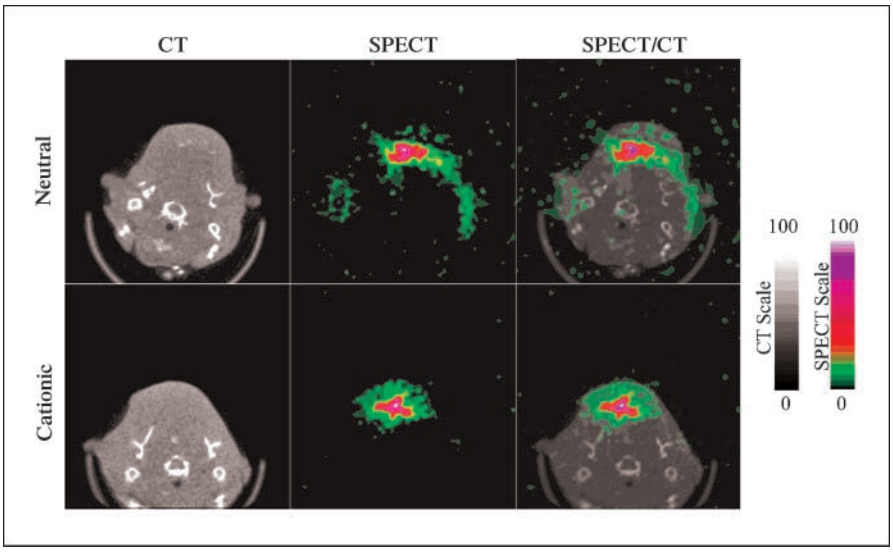

Fig. 3. Micro-CT, pinhole-collimator SPECT, and fusion images of tumor-bearing rats acquired at 20 h postintratumoral injection of ^{186}Re-neutral-liposomes (*top*) and ^{186}Re-cationic-liposomes (*bottom*). The pinhole-collimator SPECT images were focused on the tumor in each animal. The color scale shows the SPECT and CT values from 0 to maximum expressed with an arbitrary 100. The SPECT pixel values beyond the color range of the map are shown in white. The animal injected with ^{186}Re-cationic-liposomes showed more uniform and focused liposome distribution where the SPECT/CT fusion image illustrates very little activity outside of the tumor area. However, the animal injected with ^{186}Re-neutral-liposomes showed wide and dispersed activity distribution, especially the bilateral distribution of the ^{186}Re-liposomes along the lateral aspects of the torsal and forelimbs.

steadily lost weight between day 1 and day 4 and began to gain weight consistently from day 5 until the end of the 35-day study. When comparing the therapy groups with their corresponding control groups, the progression of their growth curves is almost identical. The short recovery period for the therapy groups supports the notion that the intraoperative injection of ^{186}Re-liposomes has minimal systemic side effects.

The ^{186}Re-liposome therapy groups and their respective control groups showed no signs of bleeding tendencies, and the platelet counts for the therapy groups lay mostly within the range of their respective control groups. Furthermore, no animals showed signs of infection following surgery. The WBC count for both control groups (Fig. 5B) showed a stable WBC count for 15 days. The therapy rats displayed a sustained increase in WBC count for 15 days. Their WBC count eventually decreased to within the reference range (19). However, it is important to note that the ^{186}Re-neutral-liposome group showed persistently higher WBC count beyond day 14 compared with its cationic counterpart. This is most likely due to the higher tendency of neutral liposomes for systemic spread.

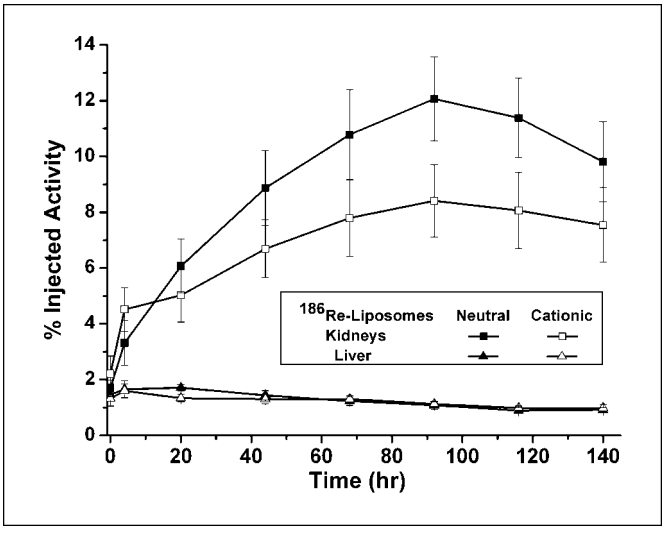

Fig. 4. Percent injected activity at different times in liver and kidneys. ^{186}Re activity was most likely renally excreted.

Toxicities. The most common side effect was the poor wound healing at the incision site. Half of the animals from each ^{186}Re-liposome therapy group experienced wound dehiscence even with meticulously placed interrupted sutures. This is expected to be contributed by the prolonged irradiation of the skin. Furthermore, four of the eight ^{186}Re-neutral-liposome rats presented with superficial skin ulceration (<4 mm in diameter) on the lateral aspects of the upper forelimbs at about day 14 and healed by day 20, which was not observed in the ^{186}Re-cationic-liposome animals or the control groups.

In terms of gastrointestinal symptoms, animals from both therapy groups showed loose and watery stools during the 1st week after therapy, and most rats began to excrete normal stools by week 2.

Histopathology. From H&E histopathology slides, control tumors (Fig. 6A) showed basophilic-stained cancer cells partitioned into lobules by the stroma and extracellular matrix. Each lobule has a central necrotic region and a periphery of expanding cancer cells. In comparison, animals from the therapy groups had tumors with multiple regions of extensive necrosis and interweaving granulation tissue (Fig. 6B). Most tumors only maintained a thin periphery of viable cancer cells. Furthermore, most ^{186}Re-treated tumors showed disintegration of the lobules and stroma and extracellular matrix disruption. Although the remaining tumors from successfully treated therapy animals showed areas of basophilic tumor cells, it is difficult to assess whether these cells are still viable tumor cells or dead cells from the basic H&E stain. Special histochemical stains will be helpful in determining the status of these remaining cells. There were no identifiable histopathologic differences in the kidney, liver, and spleen between control and therapy rats.

Discussion

Approximately 50% of the patients diagnosed with HNSCC present with stage III or IV disease (1). Despite aggressive surgery and postoperative radiation therapy, long-term survival remains low (2), and the majority of treatment failures are due

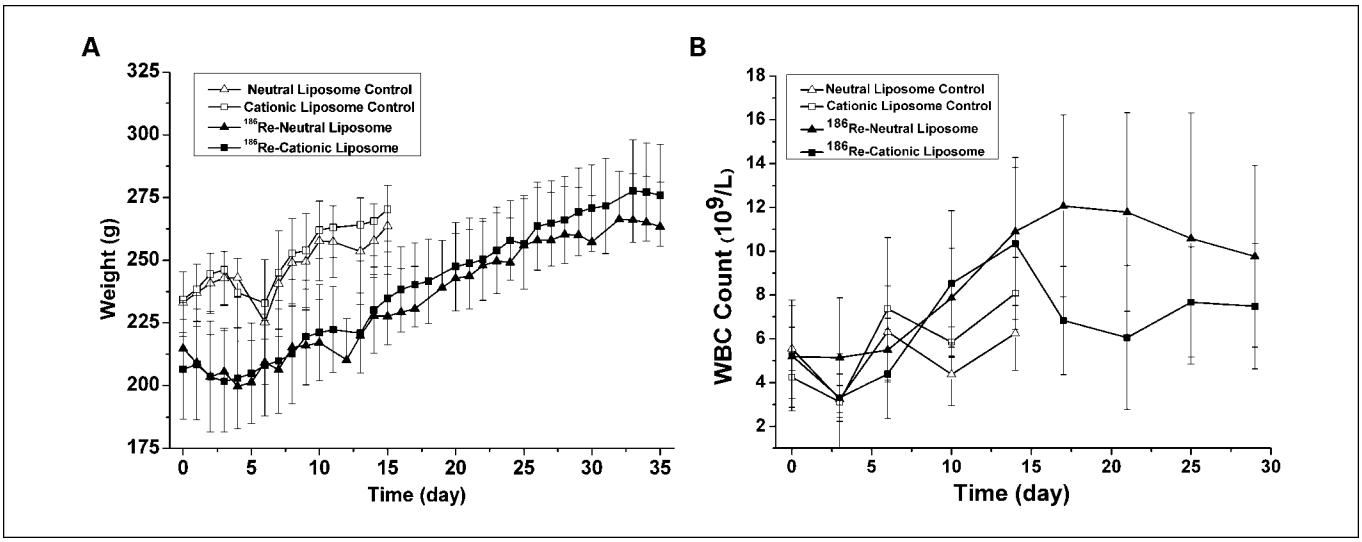

Fig. 5. Posttherapy body weight change and WBC count trend. Both control groups and therapy groups showed consistent body weight growth after surgery (*A*). When the control group and therapy group of the same formulation are compared, there is no significant difference in body weight growth ($P > 0.05$) between groups, indicating their minimal toxicity. The WBC count (10^9/L) of both control groups and therapy groups are shown (*B*). Both control groups showed stable WBC count for 15 d. The therapy rats displayed a sustained increase in WBC count from day 3 to day 14, which eventually decreased to within the reference range.

to locoregional recurrence (20). Furthermore, the recurrence rate becomes even higher when the anatomic limitations of the head and neck and the existing comorbidities preclude complete surgical resection, leaving patients with positive surgical margins (21). For these patients, radiation and/or chemotherapy become their only chance for cure (20). The modern evolution of radiation therapy for head and neck cancer, either as a single modality or as combination therapy with chemotherapy, centers on providing the maximum amount of dose to achieve local control while minimizing normal tissue toxicity. Radiation therapy is typically delivered through high-energy external beam radiation to irradiate the cancerous tissue. Yet, due to the close proximity of critical organs to the tumor, delivering the therapeutic dose of irradiation is often impossible without causing serious complications even with technological advancements in radiation dose distribution, such as intensity-modulated radiation therapy (22–24).

An alternative to surgery and radiotherapy is the integration of chemotherapy as induction or concurrent therapy to utilize the synergistic effects of chemoradiotherapy (25–27). High rates of locoregional control and organ preservation were achieved in a number of studies; however, these intense combination therapies are hampered by their dose-limiting

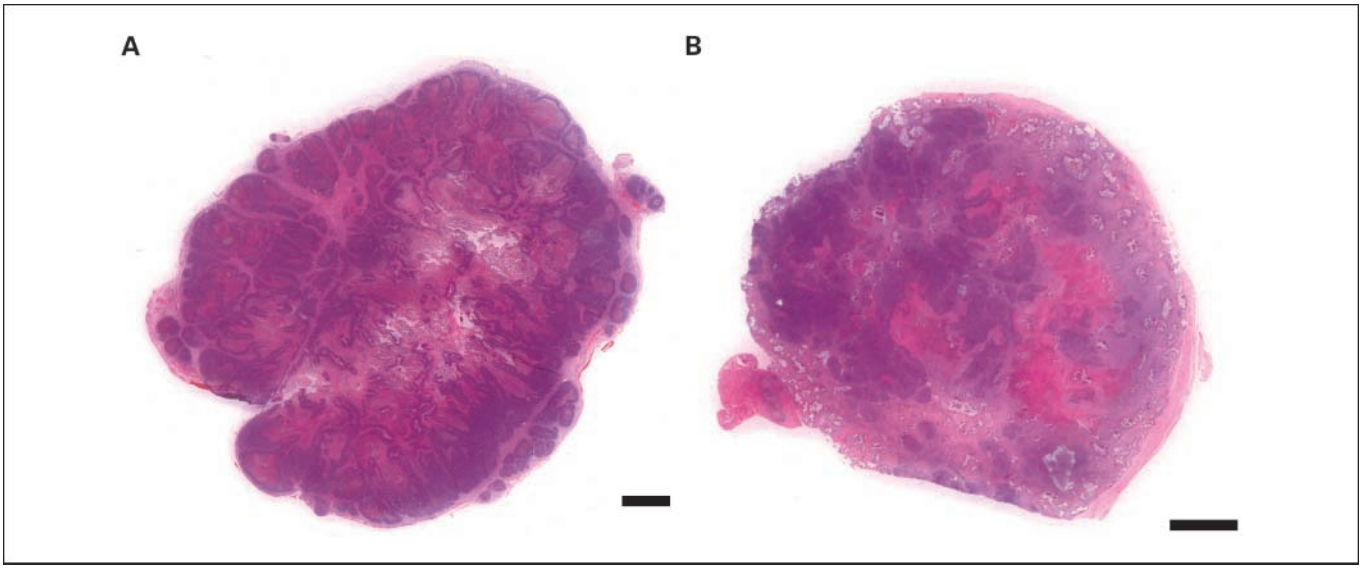

Fig. 6. Low-resolution–scanned H&E-stained section of a typical control animal tumor and a typical ^{186}Re-liposome–treated tumor. Bar, 2 mm. In the control tumor (*A*), the lobules of tumor cells are separated by interlined stroma and extracellular matrix. The ^{186}Re-liposome–treated tumor (*B*) typically showed extensive disruption of the normal stroma and extracellular matrix. There is also loss of clear division between the lobules of tumor cells.

toxicity with systemic administration. Furthermore, in an intratumoral environment, such as HNSCC, high interstitial pressure and the presence of viable tumor cells in the highly necrotic and avascular areas of the tumor render the uniform spread of chemotherapy agents difficult (28).

With the above considerations in mind, direct intratumoral drug administration in advanced HNSCC with positive margins has clear appeal by immediately achieving high drug concentration at the target site and avoiding the associated side effects of external beam radiation or systemic chemotherapy. Direct injection can deliver drugs into areas of the tumor that have high interstitial pressure and large areas of avascular necrosis. However, if free chemotherapy drugs or radionuclides were to be injected into the tumor, they would be cleared immediately. Thus, liposomes are particularly useful as nanoparticle carriers of therapeutic agents for local administration in HNSCC because of the increased local retention rates of the therapeutic agents. Due to the enhanced permeability and retention effect and the lack of a developed lymphatic system in solid tumors, the use of liposomes can further improve the retention rate of the encapsulated agent (9, 10).

Current investigations on locoregional application of liposomes include encapsulating liposomes with chemotherapeutic agents (29), genes (30), and radionuclides (12, 13). These are all feasible options to treat HNSCC locally; however, chemotherapy and gene therapy share some fundamental weaknesses. First, they both require direct interaction with the cell and, second, it is difficult to assess the intratumoral distribution of these agents without an imaging technique. Liposomal radionuclides, on the other hand, do not require a homogeneous distribution because β-emitting radionuclides (such as ^{186}Re) can provide remote killing of the cancer cell, and imaging techniques allow full assessment of the biodistribution of these agents locoregionally and systemically.

Thus far, no therapy study has been done with liposomal radionuclides. Harrington et al. (11) and Bao et al. (12) have both shown high local retention rates in HNSCC animal models. However, to treat positive margins in an intraoperative setting in which the tumor is partially resected could lead to different pharmacokinetics compared with injecting liposomal radionuclides into an intact tumor. Generally speaking, intratumoral injection of liposomal radionuclide without surgery is associated with a high immediate clearance rate and a slower phase I or phase II (if applicable) clearance rate (12). However, the postoperative inflammation and the destruction of the vasculature during surgery should reduce the immediate clearance rate (31). Data from this study (Table 2) showed low immediate clearance for both ^{186}Re-neutral-liposomes and ^{186}Re-cationic-liposomes at 13.8% and 18.4%, respectively. The long phase I half-clearance times of 48.95 and 42.04 hours for the ^{186}Re-neutral-liposomes and ^{186}Re-cationic-liposomes, respectively, also translate into high locoregional retention rate once the immediate clearance has passed. These data support the notion that the intraoperative injection of liposomal radionuclide leads to higher retention compared with direct intratumoral injection without surgical resection.

The high locoregional retention rate led to excellent therapeutic results. In this study, we were able to deliver 801.9 ± 184.9 and 617.9 ± 187.0 Gy doses of radiation, respectively, over 140 hours for the ^{186}Re-cationic-liposome and the ^{186}Re-neutral-liposome groups. At the end of the 35-day study, only one animal injected with ^{186}Re-neutral-liposomes and two animals injected with ^{186}Re-cationic-liposomes showed apparent regrowth. The final tumor volumes for the ^{186}Re-neutral-liposome group and ^{186}Re-cationic-liposome group were only 25.6 ± 21.8% and 28.5 ± 32.2%, respectively, of the initial tumor volume. The discrepancy between the final tumor size and the number of recurrent tumors for the ^{186}Re-neutral-liposome group and the ^{186}Re-cationic-liposome group is most likely the result of the actual microenvironment and macroenvironment of the specific tumor.

The tumoricidal effect of ^{186}Re-liposomes can also be shown from the histopathology studies. Control tumor sections had intact stroma and extracellular matrix partitioning tumor cells into distinct lobules; however, treated tumor samples typically displayed disruption of the stroma and extracellular matrix that is vital for the survival and growth of tumor cells by releasing tumor growth factors and nutrients (32, 33). The combination of surgical resection and irradiation from liposomal therapeutic radionuclides synergistically disrupt the macroenvironment and microenvironment of the tumor. Furthermore, surgery reinforces the efficacy of radiation by exposing hypoxic tumor cells to oxygen; it is well known that hypoxia limits the tumoricidal effects of radiation (34). The above reasons make this intraoperative injection of liposomal therapeutic radionuclides a particularly effective treatment option in a setting of positive surgical margin in advanced HNSCC.

Liposomal radionuclide therapy cannot be considered a feasible treatment option if the associated side effects are unacceptable. In this study, all side effects were acute and transient, and no complications were observed. For the therapy group animals, there is initial weight loss and loose stools that occurred in the 1st week. At approximately the end of week 1, all the animals began to show consistent weight gain and normal stools, similar to the control animals. From the dermatologic standpoint, half of the animals from each therapy group showed poor wound healing. This mainly contributed to the prevention of epithelialization by radiation damage. With deeper-seeded tumor and thicker skin, humans should experience a less-pronounced effect. A therapy group–specific dermatologic side effect was superficial skin ulcerations on the lateral aspects of the upper forelimbs observed only in four of the eight ^{186}Re-neutral-liposome rats. The skin ulcerations presented at about day 14 and healed by day 20. From the SPECT/CT fusion images in Fig. 3, we noticed that the ^{186}Re-neutral-liposomes tended to spread into the lateral aspects of the torsal and forelimb area. This behavior emerges as a potential advantage in applying ^{186}Re-neutral-liposomes for the simultaneous treatment of microscopic disease around the locoregional area. From a hematologic standpoint, Fig. 5B illustrates that the ^{186}Re-liposome–treated animals only showed a slight increase in WBC count compared with the animals that received surgical resection only. WBC levels for all control and therapy animals eventually settled within their age-appropriate normal levels (19).

Overall, the data presented in this study open new avenues in the treatment of unresectable advanced HNSCC. For future clinical studies, patients will undergo surgery in an attempt to achieve maximal resection. When maximal resection has been achieved, the ^{186}Re-liposomes would be injected into the

positive margin and/or around the tumor bed. For follow-up testing, we could use positron emission tomography, CT, or magnetic resonance imaging to check for recurrences.

Disclosure of Potential Conflicts of Interest

No potential conflicts of interest were disclosed.

References

1. Kies MS, Bennett CL, Vokes EE. Locally advanced head and neck cancer. Curr Treat Options Oncol 2001; 2:7–13.
2. Vokes EE, Weichselbaum RR, Lippman SM, Hong WK. Head and neck cancer. N Engl J Med 1993;328:184–94.
3. Chen TY, Emrich LJ, Driscoll DL. The clinical significance of pathological findings in surgically resected margins of the primary tumor in head and neck carcinoma. Int J Radiat Oncol Biol Phys 1987;13:833–7.
4. Haque R, Contreras R, McNicoll MP, Eckberg EC, Petitti DB. Surgical margins and survival after head and neck cancer surgery. BMC Ear Nose Throat Disord 2006;6:2.
5. Vokes EE. Current treatments and promising investigations in a multidisciplinary setting. Ann Oncol 2005;16 Suppl 6:vi25–30.
6. Cooper JS, Pajak TF, Forastiere AA, et al. Postoperative concurrent radiotherapy and chemotherapy for high-risk squamous-cell carcinoma of the head and neck. N Engl J Med 2004;350:1937–44.
7. Bernier J, Domenge C, Ozsahin M, et al. Postoperative irradiation with or without concomitant chemotherapy for locally advanced head and neck cancer. N Engl J Med 2004;350:1945–52.
8. Adelstein DJ, Li Y, Adams GL, et al. An intergroup phase III comparison of standard radiation therapy and two schedules of concurrent chemoradiotherapy in patients with unresectable squamous cell head and neck cancer. J Clin Oncol 2003;21:92–8.
9. Torchilin VP. Targeted pharmaceutical nanocarriers for cancer therapy and imaging. AAPS J 2007;9:E128–47.
10. Greish K. Enhanced permeability and retention of macromolecular drugs in solid tumors: a royal gate for targeted anticancer nanomedicines. J Drug Target 2007;15:457–64.
11. Harrington KJ, Mohammadtaghi S, Uster PS, et al. Effective targeting of solid tumours in patients with locally advanced cancers by radiolabelled pegylated liposomes. Clin Cancer Res 2001;7:243–54.
12. Bao A, Phillips WT, Goins B, et al. Potential use of drug carried-liposomes for cancer therapy via direct intratumoral injection. Int J Pharm 2006;316:162–9.
13. Bao A, Goins B, Klipper R, Negrete G, Phillips WT. ^{186}Re-liposome labeling using ^{186}Re-SNS/S complexes: *in vitro* stability, imaging, and biodistribution in rats. J Nucl Med 2003;44:1992–9.
14. Stewart JCM. Colorimetric determination of phospholipids with ammonium ferrothiocyanate. Anal Biochem 1980;104:10–4.
15. Bao A, Phillips WT, Goins B, et al. Setup and characterization of a human head and neck squamous cell carcinoma xenograft model in nude rats. Otolaryngol Head Neck Surg 2006;135:853–7.
16. Weber DA, Eckerman KF, Dillman LT, Ryman JC. MIRD: Radionuclide data and decay schemes. Society of Nuclear Medicine. Reston (VA): 1989. p. 328–9.
17. Zweit J. Radionuclides and carrier molecules for therapy. Phys Med Biol 1996;41:1905–14.
18. Pauwels S, Barone R, Walrand S, et al. Practical dosimetry of peptide receptor radionuclide therapy with ^{90}Y-labeled somatostatin analogs. J Nucl Med 2005; 46 Suppl 1:92–8S.
19. Vos JG, Kreeftenberg JG, Kruijt BC, Kruizinga W, Steerenberg P. The athymic nude rat. II. Immunological characteristics. Clin Immunol Immunopathol 1980;15: 229–37.
20. Grimard L, Esche B, Lamothe A, Cygler J, Spaans J. Interstitial low-dose-rate brachytherapy in the treatment of recurrent head and neck malignancies. Head Neck 2006;28:888–95.
21. Nag S, Koc M, Schuller DE, Tippin D, Grecula JC. Intraoperative single fraction high-dose-rate brachytherapy for head and neck cancers. Brachytherapy 2005;4:217–23.
22. Emami B, Lyman J, Brown A. Tolerance of normal tissue to therapeutic irradiation. Int J Radiat Oncol Biol Phys 1991;21:109–22.
23. Lee N, Puri DR, Blanco AI, Chao KS. Intensity-modulated radiation therapy in head and neck cancers: an update. Head Neck 2007;29:387–400.
24. Xia P, Fu KK, Wong GW, Akazawa C, Verhey LJ. Comparison of treatment plans involving intensity-modulated radiotherapy for nasopharyngeal carcinoma. Int J Radiat Oncol Biol Phys 2000;48:329–37.
25. Adelstein DJ, Sharan VM, Earle AS, et al. Simultaneous versus sequential combined technique therapy for squamous cell head and neck cancer. Cancer 1990; 65:1685–91.
26. Calais G, Alfonsi M, Bardet E, et al. Randomized trial of radiation therapy versus concomitant chemotherapy and radiation therapy for advanced-stage oropharynx carcinoma. J Natl Cancer Inst 1999;91:2081–6.
27. Forastiere AA, Goepfert H, Maor M, et al. Concurrent chemotherapy and radiotherapy for organ preservation in advanced laryngeal cancer. N Engl J Med 2003;349:2091–8.
28. Jain RK. Delivery of molecular and cellular medicine to solid tumors. Adv Drug Deliv Rev 2001;46: 149–68.
29. Castro DJ, Sridhar KS, Garewal HS, et al. Intratumoral cisplatin/epinephrine gel in advanced head and neck cancer: a multicenter, randomized, double-blind, phase III study in North America. Head Neck 2003; 25:717–31.
30. Villaret D, Glisson B, Kenady D, et al. A multicenter phase II study of tgDCC-E1A for the intratumoral treatment of patients with recurrent head and neck squamous cell carcinoma. Head Neck 2002;24:661–9.
31. Harrington KJ, Rowlinson-Busza G, Syrigos KN, et al. Pegylated liposome-encapsulated doxorubicin and cisplatin enhance the effect of radiotherapy in a tumor xenograft model. Clin Cancer Res 2000;6:4939–49.
32. Proia DA, Kuperwasser C. Stroma: tumor agonist or antagonist. Cell Cycle 2005;4:1022–5.
33. Anderson AR, Weaver AM, Cummings PT, Quaranta V. Tumor morphology and phenotypic evolution driven by selective pressure from the microenvironment. Cell 2006;127:905–15.
34. Hoogsteen IJ, Marres HA, Bussink J, van der Kogel AJ, Kaanders JH. Tumor microenvironment in head and neck squamous cell carcinomas: predictive value and clinical relevance of hypoxic markers. A review. Head Neck 2007;29:591–604.